

1 **Motion synchronisation patterns of the carotid atheromatous**
2 **plaque from B-mode ultrasound**

3 Spyretta Golemati^{1,2,*}, Eleni Patelaki¹, Aimilia Gastounioti³, Ioannis Andreadis¹,
4 Christos D. Liapis⁴, Konstantina S. Nikita¹

5
6 ¹Biomedical Simulations and Imaging Lab., School of Electrical and Computer
7 Engineering, National Technical University of Athens, Athens, Greece

8 ²Medical School, National and Kapodistrian University of Athens, Athens, Greece

9 ³Department of Radiology, University of Pennsylvania, Philadelphia, USA

10 ⁴Attikon University General Hospital, Medical School, National and Kapodistrian
11 University of Athens, Athens, Greece

12

13

14 Contact information:

15 Spyretta Golemati

16 Intensive Care Unit, Evangelismos Hospital, Ipsilandou 45-47, Athens 10675, Greece

17 sgolemati@med.uoa.gr

18 tel.: +302132043633

19

20 **Asynchronous movement of the carotid atheromatous plaque from B-mode**
21 **ultrasound has been previously reported, and associated with higher risk of stroke,**
22 **but not quantitatively estimated. Based on the hypothesis that asynchronous**
23 **plaque motion is associated with vulnerable plaque, in this study, synchronisation**
24 **patterns of different tissue areas were estimated using cross-correlations of**
25 **displacement waveforms. In 135 plaques (77 subjects), plaque radial deformation**
26 **was synchronised by approximately 50% with the arterial diameter, and the mean**
27 **phase shift was 0.4 s. Within the plaque, the mean phase shifts between the**
28 **displacements of the top and bottom surfaces were 0.2 s and 0.3 s, in the radial**
29 **and longitudinal directions, respectively, and the synchronisation about 80% in**
30 **both directions. Classification of phase-shift-based features using Random Forests**
31 **yielded Area-Under-the-Curve scores of 0.81, 0.79, 0.89 and 0.90 for echogenicity,**
32 **symptomaticity, stenosis degree and plaque risk, respectively. Statistical analysis**
33 **showed that echolucent, high-stenosis and high-risk plaques exhibited higher**
34 **phase shifts between the radial displacements of their top and bottom surfaces.**
35 **These findings are useful in the study of plaque kinematics.**

36

37 **Introduction**

38 The carotid atheromatous plaque is a lesion of the carotid artery wall and typically
39 consists of a fibrous cap (mostly smooth muscle cells, collagen and elastic fibers) of
40 varying thickness and a lipid core (mostly cholesterol and cellular debris). In cases of
41 advanced degeneration, plaque lesions present a more complicated structure,
42 including calcification, intraplaque hemorrhage and ulceration¹ and narrow the
43 arterial lumen, obstructing blood flow and oxygen supply to the brain. More severe
44 damage may be caused by vulnerable plaques, i.e. plaques prone to rupture. These
45 are strongly associated with the formation of blood clots and the release of plaque
46 fragments into the systemic circulation, which may cause a cerebrovascular event,
47 such as stroke or transient ischemic attack (TIA)². Given the substantial burden of
48 stroke (15 million people worldwide suffer a stroke annually, of whom 5 million die
49 and 5 million are left permanently disabled³, investigating the behaviour of carotid
50 plaque towards improving stroke prevention is of utmost importance.

51 Ultrasound imaging is the preferred imaging modality for the diagnosis of carotid
52 atheromatous plaque, owing to a number of advantages, including noninvasiveness,
53 bedside availability, short examination times, lack of radiation exposure, and low
54 cost⁴. Currently, clinical management of carotid plaque is based on the degree of
55 stenosis, i.e., the percentage of lumen area occupied by atheromatous material, and
56 the prior occurrence of symptoms⁵. Although the degree of stenosis is a validated
57 marker for management of carotid plaques, some studies have indicated that a high
58 degree of stenosis is not necessarily related to a high risk of a cerebrovascular
59 event^{6,7}. These facts indicate that there is room for improving the current clinical

60 scheme for assessing plaque vulnerability, possibly through the identification of
61 noninvasive, low-cost and reliable imaging markers for predicting strokes⁸.

62 For instance, carotid motion analysis estimated with ultrasound image sequences
63 has gained increasing attention as a potential index of plaque vulnerability⁹⁻¹².

64 Motion analysis can be defined as the estimation of arterial tissue displacement
65 during one or more cardiac cycles. It has been shown that carotid atheromatous
66 plaque performs a complex, multidirectional, often periodic, motion during the
67 cardiac cycle¹³. Despite the technical challenges, such as the low image resolution in
68 ultrasound imaging and the complexity of the local tissue geometry and mechanics,
69 several studies have suggested a number of kinematic and strain indices associated
70 with plaque rupture risk¹⁴.

71 A number of efforts have focused on motion of non-atheromatous segments of
72 the arterial wall in normal^{15,16} and pathological conditions, such as hypertension,
73 diabetes and coronary artery disease^{17,18}, as well as the motion of the wall adjacent
74 to carotid plaque^{12,16,19,20}. These studies have studied the expected cyclical motion in
75 the radial direction and have also identified a longitudinal component of wall
76 motion. It has also been observed that decreased longitudinal movement of the
77 common carotid artery is associated with higher plaque burden²⁰. Significantly lower
78 amplitudes of both radial and longitudinal displacements have been found in older
79 diabetic subjects, compared to healthy young adults¹⁸. Recently, the feasibility of
80 assessing tissue motion inhomogeneities was demonstrated along with their
81 association with the presence of coronary artery disease²¹. Blood pressure has been
82 positively correlated with common carotid artery displacement¹⁷. Other studies have
83 suggested that the severity of carotid stenosis is associated to axial wall stresses and

84 accelerations¹⁹, as well as to the presence of an anterograde component in the
85 longitudinal direction of wall motion¹².

86 Related studies have proposed various metrics to quantify plaque motion
87 patterns, including statistical measures of velocities, motion amplitudes and diastole-
88 to-systole displacements of the entire plaque area during the cardiac cycle^{11,13},
89 maximal (discrepant) surface velocities^{9,22} and displacement vector maps²³. A group
90 of studies have also qualitatively described the so called “jellyfish sign”
91 phenomenon, according to which the carotid plaque surface rises and falls in a
92 manner inconsistent with arterial pulsatile wall motion²⁴⁻²⁶. Other similar
93 phenomena include motion of intraplaque contents²⁷, mobility at the edge of the
94 plaque, mobility in all parts of the plaque and mobility at the bottom of an ulcer on
95 the plaque²⁶. Studies have also investigated tissue strain, i.e. the change of
96 displacement with respect to some initial reference status^{10,28-32}. These studies have
97 converged to the general conclusion that softer, echolucent plaques undergoing
98 higher strains tend to be more prone to rupture and they are associated with poorer
99 patient cognition. The concept of concordant and discordant motion was recently
100 introduced to describe the spread of motion of different plaque areas³³.

101 Among the investigated phenomena, relative motion between the plaque and
102 the adjacent wall^{13,24-26}, as well as within the plaque itself^{26,27} has been reported in
103 some studies. The patterns of synchronisation of such relative movements have only
104 been estimated qualitatively in a few studies²⁴⁻²⁶ and have shown that asynchronous
105 motion of the plaque relative to the adjacent wall is associated with plaque
106 instability and stroke recurrence.

107 To the best of our knowledge, there is no study focused on investigating
108 synchronisation patterns of carotid plaque motion in an automated and quantitative
109 way. Therefore, the purpose of this study was to quantify synchronisation patterns
110 of the carotid plaque, in relation to its adjacent wall and within itself, and investigate
111 potential associations of these synchronisation patterns with different plaque
112 phenotypes, including echogenicity, stenosis degree, patient symptoms and plaque
113 risk. The major contributions of this work are to (a) suggest a systematic approach
114 for assessing such patterns, (b) provide specific numerical indices (measured in
115 seconds) for the related phenomena, i.e. the phase shifts between plaque and wall,
116 and within plaque in radial and longitudinal directions, and (c) evaluate the derived
117 indices in different plaque phenotypes, based on the hypothesis that asynchronous
118 plaque motion is associated with phenotypes characterising vulnerable plaque,
119 namely echolucency, symptomaticity, high stenosis degree and high risk. These
120 contributions will provide new knowledge about plaque biomechanics, which is
121 important and necessary for future studies, including prognostic follow-up
122 assessments.

123

124 **Materials and Methods**

125 *Dataset*

126 Seventy seven consecutive patients (59 men, 18 women) with carotid
127 atherosclerosis were included in the study, free from comorbidities, including heart
128 failure, liver dysfunction, cancer, chronic diseases etc. Subjects were on statin-based,
129 anti-platelet and lipid-lowering medication. The dataset included 18 symptomatic
130 patients (31 plaques, degrees of stenosis $66\% \pm 29\%$), 57 asymptomatic patients (98

131 plaques, degrees of stenosis $73\% \pm 22\%$ and 2 patients (6 plaques) whose
132 symptomaticity or stenosis degree was unknown; the latter were only included in
133 the association-with-echogenicity study. The symptomatic subjects, for whom only
134 the ipsilateral artery was studied, had experienced a stroke or a TIA, within 6 months
135 prior to the examination. A number of asymptomatic subjects had plaque in both the
136 right and left carotids and in both types of subjects more than one plaque may be
137 present in an artery (tandem lesions); tandem lesions were treated as separate
138 plaques. The patients' ages were 70 ± 9 years (range 43-85 years), and their stenosis
139 degrees $75\% \pm 17\%$ (range 20-99%), based on Doppler ultrasound measurements.

140 B- mode ultrasound images were acquired in longitudinal section using a LOGIQ
141 Book (GE Medical Systems, Milwaukee, WI, USA) scanner and a linear array 4-10
142 MHz transducer. Subjects were examined in a supine position, with a slight backward
143 inclination of the head, towards the opposite side of the carotid under examination.
144 Patients rested for at least 5 minutes before the examination, to stabilise their heart
145 rate and blood pressure. To minimise movements due to factors other than
146 haemodynamic forces, the operator held the transducer as stable as possible,
147 exerting minimal pressure, and the patients were asked to breath-hold during
148 recordings. Scanner and transducer settings included a high dynamic range (60 or 75
149 dB) and zero persistence, and 10 MHz centre frequency. At least three cardiac cycles
150 were recorded at a rate of 25 frames/s. Image resolution was 12 pixels/mm in the
151 radial and longitudinal directions. The room temperature was kept constant at 26°C .

152 All ultrasound examinations were performed by 4 experienced physicians in the
153 Vascular Surgery Department of the University Hospital "ATTIKON", Athens, Greece.
154 Data collection was approved by the ATTIKON hospital institutional review board and

155 all subjects included in the study gave their informed consent to the scientific use of
156 the data. The methods were carried out in accordance with the relevant guidelines
157 and regulations.

158

159 *Estimation of plaque motion synchronisation patterns*

160 Plaque motion synchronisation patterns relative to the adjacent normal wall as
161 well as within the plaque were estimated through cross-correlations of pairs of
162 waveforms representing displacements of plaque and wall tissue.

163 *1) Basic principles of cross-correlation.* Cross-correlation r_d is a measure of
164 similarity of two signals in the form of time series, $x(i)$ and $y(i)$, where $i =$
165 $1, 2, \dots, N$ denotes time points, as a function of the displacement d (also known as
166 lag) of one relative to the other³⁴. If cross-correlation is calculated for all lags
167 $d = 0, 1, \dots, N - 1$, then the resulting cross-correlation sequence is twice as long as
168 that of the correlated series. The following formula for cross-correlation was used:

169

$$r_d = \frac{\sum_i [(x(i) - m_x)(y(i - d) - m_y)]}{\sqrt{\sum_i (x(i) - m_x)^2} \sqrt{\sum_i (y(i) - m_y)^2}}$$

170

171 where m_x and m_y are the mean values of signals $x(i)$ and $y(i)$, respectively. The
172 denominator in this formula serves to normalise the correlation coefficients, so that
173 the cross-correlation is 1, for lag equal to 0. The subtraction of the mean values
174 m_x and m_y from the signals allows signals from different subjects to be comparable.
175 The length N of the signals coincides with the maximum duration of the ultrasound
176 recording in each case.

177 If the peaks (or the troughs) of two time-varying signals coincide in time, their
178 cross-correlation has a high positive value. These signals are considered
179 synchronous, or in-phase, or with a 0° phase shift. If the peaks of one signal coincide
180 in time with the troughs of the other signal, their cross-correlation has a high
181 negative value. These signals are considered asynchronous, or out-of-phase, or with
182 a 180° phase shift. A cross-correlation value equal to 0 indicates uncorrelated signals.

183 *2) Description of methodology.* The main steps of the methodology are described
184 below and illustrated in Fig.1.

185 *A - Selection of regions of interest (ROIs).* For each plaque image sequence
186 (video), an experienced physician marked manually in the first frame the following
187 four ROIs: the posterior and anterior wall-lumen interfaces (PWL and AWL,
188 respectively), and the plaque top and bottom surfaces (PTS and PBS, respectively)
189 (Fig.1a). PWL and AWL were selected on the normal, i.e. non-atheromatous, arterial
190 wall, adjacent to the plaque.

191 *B - Motion estimation of selected ROIs.* The radial and longitudinal positions of all
192 pixels included in the selected ROIs were estimated across all frames with an
193 adaptive block-matching algorithm, which incorporates Kalman filtering³⁵. This
194 algorithm was evaluated in an *in silico* framework consisting of 13 simulated
195 sequences, and has been shown to be accurate and robust in motion tracking of the
196 arterial wall from B-mode ultrasound images¹³. For each ROI, $1.6 \times 1 \text{ mm}^2$ reference
197 blocks were selected in the first frame, centred at ROI pixels. Fig.1b shows examples
198 of selected ROIs (AWL, PWL, PTS, PBS) for a diastolic, an intermediate and a systolic
199 frame and of the sequence.

200 *C - Waveforms extracted from motion analysis.* ROI positions were used to
201 estimate six sets of waveforms for each plaque:
202 (i) wall diameter, which was selected as the most representative waveform, i.e. the
203 one in which the most clear cyclic motion was observed, among the distances of
204 vertical pairs of AWL and PWL pixels,
205 (ii) radial displacements of all PTS pixels, namely their radial positions along
206 consecutive frames,
207 (iii) longitudinal displacements of all PTS pixels, namely their longitudinal positions
208 along consecutive frames,
209 (iv) radial displacements of all PBS pixels,
210 (v) longitudinal displacements of all PBS pixels, and
211 (vi) radial distances of PTS and PBS pixel pairs, defined as the absolute differences of
212 waveforms (ii), (iv) across vertical pixel pairs.

213 Twenty five pixels from the right and 25 from the left edge of the plaque PTS and
214 PBS were removed to ensure that only plaque pixels, and no normal (non-plaque)
215 wall area, were included in the analysis. The number of removed pixels (25) was
216 heuristically determined, following visual inspection and testing. Fig.1c shows
217 examples of interrogated waveforms.

218 A high-pass 4th order Butterworth filter with a cutoff frequency of 0.6 Hz was
219 applied to the displacement waveforms³⁶, so as to remove unwanted offsets or
220 abrupt fluctuations present in the low-frequency band. The cutoff value was selected
221 to ensure that heart rates above approximately 40 beats per minute remain
222 unaffected after filtering. Independent component analysis (ICA) demonstrated that

223 the suggested methodology is robust against external motion (Supplementary
224 methods).

225 *D - Calculation of cross-correlations.* Three types of cross-correlations were
226 calculated using the previously described waveforms:

227 a) Cross-correlation 1 (CC1): Radial deformation of the plaque with wall diameter, i.e.
228 waveforms (i) and (vi),

229 b) Cross-correlation 2 (CC2): Radial displacements of plaque top and bottom
230 surfaces, i.e. waveforms (ii) and (iv), and

231 c) Cross-correlation 3 (CC3): Longitudinal displacements of plaque top and bottom
232 surfaces, i.e. waveforms (iii) and (v).

233 CC2 and CC3 describe intra-plaque kinematics, whereas CC1 was considered, so
234 as to provide a measure with respect to a well-known arterial parameter.

235 Fig.1d shows examples of interrogated pairs of waveforms ((a)-(c), above) and
236 their corresponding cross-correlations.

237 Signals to be correlated were confined within an average cycle window,
238 estimated from the dominant frequency of the wall diameter waveform.

239 From each cross-correlation waveform, two types of measurements were
240 obtained: (a) the sign corresponding to the maximum absolute cross-correlation, and
241 (b) the corresponding lag d_{max} , in seconds (Fig.1d). For each plaque, cross-correlation
242 waveforms were produced for all PTS-PBS pairs, and the following indices were then
243 extracted:

- 244 • The synchronisation percentage, defined as the percentage of the positive
245 values present in the entire set of maximum signed cross-correlation values,
246 derived from all PTS-PBS pairs of the plaque. According to the principles of

247 cross-correlation described previously, this percentage represents the
248 proportion of plaque pairs that exhibit synchronous motion patterns for a
249 given type of cross-correlation.

- 250 • Seven statistical (histogram-based) measures (maximum-, minimum-, mean-,
251 median-value, standard deviation, skewness, and kurtosis) of the lags d_{max}
252 extracted from all PTS-PBS pairs of the plaque.

253

254 Therefore a total of 24 features were extracted for each plaque, namely 8
255 features (synchronisation percentage and 7 statistical indices) for each of the 3
256 cross-correlation types.

257

258 *Grayscale normalisation and estimation of plaque echogenicity*

259 To normalise ultrasound images according to widely accepted procedures³⁷, the
260 physician selected a region in the blood and one in the adventitia, and the median
261 pixel values of these regions (GSM_{blood} and GSM_{adv} , respectively) were set as the
262 lowest (black) and the highest (white) values in the image, respectively. Then, the
263 image grayscale intensities were linearly adjusted so that GSM_{blood} was 0, and GSM_{adv}
264 was 190³⁷.

265 An echolucent plaque is a dark appearing plaque in the ultrasound recording,
266 while an echogenic plaque is a bright appearing one³⁸. Plaque echogenicity was
267 estimated as follows: the plaque was located automatically in each frame of the
268 sequence after the first frame, using motion analysis of PBS and PTS areas, and the
269 corresponding grayscale median (GSM) values were calculated. Plaque GSM was

270 defined as the mean value of the GSMs of all frames. Echolucent plaques were
271 considered those with a $GSM < 25^{39}$ and echogenic those with $GSM \geq 25$.

272

273 *Variability study*

274 Intra and inter-observer variability were assessed by means of phase shift
275 measurements performed for plaque boundaries displaced by 0-2 pixels with respect
276 to the original (expert-annotated) ones. This experiment was designed based on the
277 assumption that different observers, or the same observer at different times,
278 produce different tissue outlines, which are displaced versions of a given contour.
279 The range of the displacements (0-2 pixels, including subpixel values) was selected
280 heuristically, based on observations that tissue outlines derived by different experts
281 were not more than 2 pixels apart. Differences between original and displaced
282 versions in all cases were assessed statistically.

283

284 *Classification & statistical analysis*

285 The four associations investigated were validated through classification schemes
286 using supervised machine learning. The purpose of classification was to evaluate the
287 overall potential of the extracted features, which, can alternatively be considered as
288 a “motion synchronisation signature”, through their association with the four clinical
289 phenotypes. Subsequently, statistical analysis was performed, to identify the
290 features with the highest discriminatory ability.

291 Feature selection was applied using Principal Component Analysis (PCA),
292 whereby the initial feature set is converted into a reduced set of linearly
293 uncorrelated features, orthogonal to each other (principal components), which

294 retains most of the initial set's variance, namely, its information content⁴⁰. For this
295 study, as many principal components as necessary were retained to cover 95% of the
296 initial set's variance.

297 Classification models for each association were implemented using the Weka
298 workbench version 3.6 (Machine Learning Group at the University of Waikato,
299 Hamilton, New Zealand)⁴¹. Among the algorithms available in Weka, the Random
300 Forest (RF) algorithm was used, due to its superior performance and its robustness
301 to overfitting⁴². The RF algorithm uses a number of parameters that need to be
302 tuned properly, before training, to avoid overfitting or underfitting. The two
303 parameters that were tuned included the number of features to be used in random
304 selection (range: 2-number of features, with a step of 1), and the number of trees to
305 be generated (range: 100-900, with a step of 200). For parameter tuning, 10-fold
306 cross-validation was used. The parameters that were tuned included the number of
307 data points, the number of features of each tree of the forest, and the number of the
308 trees that we build for the forest.

309 To address the problem of class imbalance that is present in our data, the
310 ADASYN algorithm⁴³ was applied to create synthetic samples for the minority class,
311 i.e. the class with the lowest number of cases. Of note, these synthetic samples were
312 used only for training the model, not for testing.

313 For the evaluation of each model, leave-one-out cross-validation (LOOCV) was
314 chosen, because the medium size of our dataset indicated it as the optimal choice in
315 terms of computational cost, as well as bias-variance trade-off⁴⁴.

316 To evaluate the performance of the classification models, a set of metrics was
317 calculated, including accuracy (ACC), sensitivity (SENS), specificity (SPEC), precision

318 (PREC), negative predictive value (NPV), F1 score (F1SC) and the area under the
319 Receiver Operating Characteristics (ROC) curve (AUC)⁴⁵.

320 Statistical analysis was performed using the non-parametric Wilcoxon rank sum
321 test and statistical significance was considered for a p-value equal to or lower than
322 0.05.

323 All analyses were performed using Matlab R2016a (MathWorks, Natick, MA, USA) and a
324 computer with an Intel Core i5 220 GHz CPU.

325

326 **Results**

327 Table 1 shows the performance of the RF classifier, for the four associations
328 interrogated, in terms of the evaluation metrics described in the previous section.
329 This corresponds to the overall performance of all interrogated PCA-selected
330 features.

331 Regarding the variability study, all indices were similar between the original and
332 the displaced versions. As an example, the p-values for the mean phase shifts were
333 0.46 for CC1 and CC2 and 0.39 for CC3.

334 In the following subsections detailed results are presented for the statistical
335 analysis of the entire dataset, for each of the investigated scenarios. Tables showing
336 statistical analysis results present values for synchronisation percentages and mean
337 phase shifts, even if they were not found statistically different, so as to provide a feel
338 for these measures, given they are reported for the first time.

339

340 *Association with plaque echogenicity*

341 Of the 135 plaques of the dataset, 37 were echolucent ($GSM < 25$) and 98 were
342 echogenic ($GSM \geq 25$). The stenosis degrees and ages were not statistically different in
343 the two groups (p-values=0.17 and 0.24, respectively).

344 The application of PCA identified 13 features as the principal components
345 satisfying the 95% variance coverage criterion for this association.

346 Table 2 shows the mean values and corresponding p-values of the
347 synchronisation percentages, mean phase shift values, and statistically significant
348 features for the three cross-correlation types, in echogenic and echolucent plaques.
349 As we can see, in echolucent plaques, the top plaque surface moves less

350 synchronously (with a higher phase shift) relative to the bottom surface, than in
351 echogenic plaques, in the radial direction (higher mean_{CC2} and $\text{median}_{\text{CC2}}$). Also, the
352 mean phase shifts between top and bottom surfaces of both echogenic and
353 echolucent plaques were significantly higher in the longitudinal direction, compared
354 to the radial direction.

355

356 *Association with symptomatology*

357 Of the 124 plaques used in this substudy, 93 caused a degree of stenosis higher
358 than or equal to 70%. Of these 93 high-stenosis plaques, 71 were asymptomatic and
359 22 were symptomatic. The stenosis degrees and ages were not statistically different
360 in the two groups (p -values=0.15 and 0.35, respectively).

361 The application of PCA identified 11 features as the principal components
362 satisfying the 95% variance coverage criterion for this association.

363 Table 3 shows the mean values and corresponding p -values of the
364 synchronisation percentages, mean phase shift values, and statistically significant
365 features for the three cross-correlation types, for asymptomatic and symptomatic
366 plaques. As we can see, there was no difference between symptomatic and
367 asymptomatic cases (except for 3 histogram-based features). Also, the mean phase
368 shifts between top and bottom surfaces of asymptomatic plaques were significantly
369 higher in the longitudinal direction, compared to the radial direction. Symptomatic
370 plaques did not show such difference.

371

372 *Association with stenosis degree*

373 Of the 124 plaques used in this substudy, 97 were asymptomatic. Of these 97
374 asymptomatic plaques, 26 caused a low degree of stenosis (<70%) and 71 caused a
375 high degree of stenosis ($\geq 70\%$). The ages of the patients were not statistically
376 different in the two groups (p-value=0.16). By definition, the high-stenosis group in
377 this study is the same as the asymptomatic group in the previous study.

378 The application of PCA identified 13 features as the principal components
379 satisfying the 95% variance coverage criterion, for this association.

380 Table 4 shows the mean values and corresponding p-values of the
381 synchronisation percentages, mean phase shift values, and statistically significant
382 features for the three cross-correlation types, for low- and high-stenosis plaques. As
383 we can see, in high-stenosis plaques, the top plaque surface moves less
384 synchronously (higher \max_{CC2} , higher mean_{CC2}) and less uniformly (higher stdev_{CC2})
385 relative to the bottom surface, than in low-stenosis plaques, in the radial direction.
386 Also, the mean phase shifts between top and bottom surfaces of both low- and high-
387 stenosis plaques were significantly higher in the longitudinal direction, compared to
388 the radial direction.

389

390 *Association with plaque risk*

391 Of the 124 plaques used in this substudy, 26 were low-risk and 98 were high-risk.
392 The ages of the patients were not statistically different in the two groups (p-
393 value=0.25). According to the current clinical decision-making scheme, high-risk
394 subjects are symptomatic ones with stenosis degrees $\geq 50\%$ ⁴⁶ and asymptomatic
395 subjects with stenosis degrees $\geq 70\%$ ⁴⁷; otherwise subjects are considered low-risk⁵.

396 The application of PCA identified 12 features as the principal components
397 satisfying the 95% variance coverage criterion for this association.

398 Table 5 shows the mean values and corresponding p-values of the
399 synchronisation percentages, mean phase shift values, and statistically significant
400 features for the three cross-correlation types, for low- and high-risk plaques. As we
401 can see, in high-risk plaques, the top plaque surface moves less synchronously
402 (higher $mean_{CC2}$) and less uniformly (higher $stdev_{CC2}$) relative to the bottom surface,
403 than in low-risk plaques, in the radial direction. In addition to this, most of the
404 significantly different features (3 out of 4) were derived from cross-correlation type
405 2, namely between radial motion of top and bottom plaque surfaces. Also, the mean
406 phase shifts between top and bottom surfaces of both low-risk and high-risk plaques
407 were significantly higher in the longitudinal direction, compared to the radial
408 direction.

409

410 As it can be observed, a few of the features in the previous Tables 2, 4 and 5
411 present high standard deviations, sometimes even higher than the corresponding
412 mean values ($median_{CC2}$ in Table 2, and min_{CC1} in Tables 4 and 5), indicating a high
413 inter-plaque variability, probably due to differences between subjects.

414

415 *Representative examples of cross-correlation distributions*

416 Figures 2 and 3 illustrate examples of distributions of cross-correlations of the
417 three types of cross-correlations for an echogenic, asymptomatic, low-stenosis case
418 and an echolucent, symptomatic, high-stenosis case, respectively. Cross-correlation
419 values correspond to pixels along the manually extracted plaque contour in the first
420 frame of the sequence. Videos 1 and 2 show the displacements of the interrogated
421 ROIs (AWL, PWL, PTS and PBS) in each case. Synchronisation percentages were 38%,
422 100% and 100% for CC1, CC2 and CC3, respectively, in the asymptomatic case and
423 95%, 72% and 53% for CC1, CC2 and CC3, respectively, in the symptomatic case.
424 Mean phase shifts were 0.45 s, 0.00 s and 0.04 s for CC1, CC2 and CC3, respectively,
425 in the asymptomatic case and 0.79 s, 0.33 s and 0.48 s for CC1, CC2 and CC3,
426 respectively, in the symptomatic case.

427

428 **Discussion**

429 This study showed that the synchronisation percentages in our dataset were
430 approximately 50%, 80% and 80%, for CC1, CC2 and CC3, respectively, and the mean
431 phase shifts were 0.4 s, 0.2 s and 0.3 s, respectively. To the best of our knowledge,
432 such features characterising phase shifts and synchronisation percentages of the
433 motion of carotid atheromatous plaque from B-mode ultrasound have not been
434 previously quantified. The RF algorithm yielded AUC scores of 0.81, 0.79, 0.89 and
435 0.90, for the association with echogenicity, symptomaticity, stenosis degree and
436 plaque risk, respectively. It was also observed that echolucent, high-stenosis and
437 high-risk plaques had significantly higher phase shifts between the radial

438 displacements of their top and bottom surfaces (0.23-0.26 s on average), compared
439 to echogenic, low-stenosis and low-risk plaques (0.16-0.20 s on average).

440 The interrogated phenotypes were selected on the grounds of their associations
441 with plaque vulnerability and selection of treatment. Specifically, echogenicity has
442 been associated with increased vulnerability. Symptomatic and asymptomatic
443 plaques with stenosis degrees higher than 70% are currently offered carotid
444 revascularisation⁵. Asymptomatic subjects with low- and high-stenoses are offered
445 different treatments; conservative treatment with medication for the former, while
446 carotid revascularisation for the latter⁵.

447 Feature selection identified the same set of features for most association
448 scenarios (3 out of 4, with a small differentiation for the symptomaticity scenario).
449 Also, in all association studies, NPV had the lowest value among all evaluation
450 metrics. This is expected, because the “negative” class was the minority class,
451 namely it was outnumbered by the “positive” class, therefore, this metric reflects the
452 inferiority of the “negative” class in terms of sample size. It is pointed out that 3
453 additional classifiers, besides RF, were benchmarked on the same dataset, namely
454 Multilayer Perceptron, Nearest Neighbours and Support Vector Machines (SVMs).
455 These algorithms perform supervised machine learning, i.e. their inputs and outputs
456 are known; see⁴⁸ for more information. The performances of these classifiers were
457 inferior compared to the RF algorithm.

458 Although feature selection identified 12-13 features for each association
459 scenario, statistical analysis yielded fewer features, namely 2-4 depending on the
460 scenario. This indicates that despite the relatively low number of statistically
461 significant features in a specific association, there is additional, potentially

462 discriminatory, information which is uniformly distributed among the entire set of
463 the 24 features, and is revealed with classification. The good performance of the
464 classifiers, ranging from 79% to 90%, indicates that there is sufficient information
465 present in the datasets of all association scenarios.

466 Most of the previous studies have used statistical tests to validate their
467 results^{9,13,22,25-27}, while machine learning methodologies have been introduced in
468 fewer cases^{11,30,32-24}. Specifically, Gastounioti et al.¹¹ compared multiple classifiers
469 and feature selection methods, as well as combinations of them, and concluded that
470 the SVM classifier combined with the Fisher Discriminant Ratio for feature selection
471 were optimal in discriminating symptomatic and asymptomatic patients. Meshram et
472 al.³⁰ and Wang et al.³² implemented a logistic regression classifier and ROC analysis,
473 towards correlation of plaque strain indices with patient cognitive function. Finally,
474 Ichinose et al.²⁴ implemented a multiple linear regression analysis (stepwise analysis
475 and partial least squares analysis), followed by a machine learning analysis using an
476 Artificial Neural Network based on the Log-Linearised Gaussian Mixture Network, to
477 correlate the “jellyfish sign” of motion with the presence of new lesions, detected by
478 diffusion-weighted imaging. The generation of these lesions is the most common
479 complication caused by carotid artery stenting. Machine learning is appropriate for
480 the study of complex relations, whereas statistical tests are limited to simpler cases.
481 The combination of both machine learning and statistical analysis methodologies,
482 which is implemented in the current study, allows the design of a robust, multi-level
483 validation scheme and, thus, the extraction of reliable results about the complex
484 phenomenon of plaque motion synchronisation.

485 Echolucent, high-stenosis and high-risk plaques presented significantly higher
486 phase shifts between the radial displacements of their top and bottom surfaces,
487 compared to echogenic, low-stenosis and low-risk plaques. A potential implication of
488 these findings is that asynchronous motion patterns are associated with higher
489 plaque vulnerability, given their association with its determinants, including
490 echolucency, high-stenosis and presumed high risk. These results and related
491 implications should be confirmed in follow-up studies. In contrast, statistical analysis
492 between symptomatic and asymptomatic plaques did not reveal any differences.
493 This finding may imply that echogenicity and stenosis degree hold more information
494 and, thus, are more crucial clinical parameters, than symptomaticity, as far as plaque
495 kinematics are concerned. Moreover, the significantly higher phase shifts in the
496 longitudinal direction, in the majority of interrogated groups (7 out of 8), indicate
497 more asynchronous intra-plaque motion in the longitudinal direction, than in the
498 radial direction.

499 The main findings of this research, namely that echolucent, high-stenosis and
500 high-risk plaques are characterised by higher phase shifts and, thus, less synchronous
501 motion patterns between the radial motion of their top and bottom surfaces than
502 echogenic, low-stenosis and low-risk plaques, qualitatively agree with other studies
503 on plaque kinematics. Gastouniotti et al.¹³ reported that symptomatic plaques
504 presented 37% higher radial motion range of PTS and 50% higher relative movement
505 between PTS and PBS. Moreover, Kume et al.²⁵, Ogata et al.²⁶ and Ichinose et al.²⁴
506 showed that the jellyfish sign, a pattern that characterises the asynchronous motion
507 of the plaque relative to the adjacent wall, is associated with plaque vulnerability
508 and stroke recurrence. Gastouniotti et al.⁴⁹ found that echolucent plaque segments

509 moved more intensely in the radial direction, compared to echogenic plaque
510 segments. Finally, Tat et al.¹² reported that patients with severe plaque stenosis
511 presented greater longitudinal anterograde wall motion than those with moderate
512 stenosis. In combination with our finding that high-stenosis plaques had significantly
513 higher and more dispersed phase shifts between the radial displacement of their top
514 and bottom surfaces, this suggests that irregular wall dynamics characterising high-
515 stenosis cases may be reflected not only within plaque but also in relative movement
516 with the adjacent wall.

517 This work is one of the studies demonstrating the ability to extract features
518 characterising tissue kinematics from B-mode ultrasound images. Although
519 radiofrequency ultrasound is being widely used for tissue motion and strain
520 estimation^{23,31,32}, B-mode has also been used for motion measurements^{22,24,26,29}. In
521 this work, only B-mode data were available in the commercial scanning device that
522 was used. It has been shown that radiofrequency ultrasound outperforms B-mode,
523 due to its reduced variability in cardiac strain estimation⁵⁰. A more recent study
524 however showed that local arterial characteristics can be assessed equally reliably
525 and accurately with B-mode technology⁵¹. Advantages of B-mode include relatively
526 low-cost and widespread use in clinical practice, while radiofrequency devices are
527 higher-cost and mostly used for research purposes. It is therefore important to be
528 able to extract as much information as possible from the widely available B-mode
529 devices allowing to address a wider range of clinical applications. B-mode-
530 ultrasound-based tissue kinematics could be further combined with other plaque
531 properties, such as neovascularisation and elasticity, assessed using contrast-

532 enhanced ultrasound and elastography, respectively, towards providing an overall
533 valid plaque characterisation⁵².

534 Motion of the arterial wall and plaque during the cardiac cycle is a particularly
535 complex phenomenon, resulting from the combined effect of a number of different
536 forces/stresses, including translation, rotation, shear, tethering, etc. Taking into
537 account the complexity of this phenomenon, in this study we selected to address
538 representative plaque motion patterns, namely in relation to adjacent wall as well as
539 in the radial and longitudinal directions within itself.

540 The limitations of this study include the medium size and the heterogeneity of
541 the dataset. Compared to previous studies on ultrasound-based carotid plaque
542 kinematics, in which dataset sizes ranged from 11 to 165 patients, our 77-patient
543 (135-plaque) dataset was considered adequate for benchmarking our methodology.
544 Dataset heterogeneity consists in including subjects of both gender and with lesions
545 located in both the left and right carotids. Although larger and more homogeneous
546 datasets are always desirable to reach safer conclusions, we believe that the medium
547 size of our dataset and the grouping into smaller, somewhat more homogeneous,
548 datasets has allowed us to make some reliable and interesting observations.

549 The findings presented in this study are promising for further in-depth study of
550 carotid plaque kinematics from B-mode ultrasound. Future work in this area might
551 focus on the combination of phase-shift features with other ultrasound-based
552 kinematic features towards extracting valuable information about plaque mechanics.
553 The application of the proposed classification model to substantially larger datasets,
554 including follow-up patient data, will allow the identification of potential novel
555 markers for improved risk stratification.

556 In conclusion, this study quantified synchronisation patterns of the carotid
557 atheromatous plaque from B-mode ultrasound, and associated them with
558 echogenicity, symptomaticity, stenosis degree and plaque risk. Synchronisation
559 percentages in our dataset were approximately 50%, 80% and 80% and the mean
560 phase shifts 0.4 s, 0.2 s and 0.3 s, for cross-correlation types 1, 2 and 3, respectively.
561 The RF algorithm, combined with PCA, achieved very good performance in the
562 benchmarking procedures, yielding AUC scores of 0.81, 0.79, 0.89 and 0.90, for the
563 association with echogenicity, symptomaticity, stenosis degree and plaque risk,
564 respectively. Statistical analysis showed that echolucent, high-stenosis and high-risk
565 plaques exhibited higher phase shifts between the radial displacements of their top
566 and bottom surfaces. These findings are promising for further in-depth study of
567 ultrasound-based carotid plaque kinematics, towards improving risk stratification.

568

569 **Data availability**

570 The datasets generated and analysed during the current study are available from the
571 corresponding author on reasonable request.

572

573 **References**

- 574 1 Hayward, J. K., Davies, A. H. & Lamont, P. M. Carotid plaque morphology: a
575 review. *Eur J Vasc Endovasc Surg* **9**, 368-374 (1995).
- 576 2 Howard, G. *et al.* Is blood pressure control for stroke prevention the correct
577 goal? The lost opportunity of preventing hypertension. *Stroke* **46**, 1595-1600
578 (2015).
- 579 3 McKay, J. & Mensah, G. A. *The Atlas of Heart Disease and Stroke*. (Geneva :
580 World Health Organization, [2004] ©2004, 2004).
- 581 4 Nikita, K. S. Atherosclerosis: the evolving role of vascular image analysis.
582 *Comput Med Imaging Graph* **37**, 1-3 (2013).

583 5 Liapis, C. D. *et al.* ESVS guidelines. Invasive treatment for carotid stenosis:
584 indications, techniques. *Eur J Vasc Endovas Surg* **37**, 1-19 (2009).

585 6 Naylor, A. R. Time to rethink management strategies in asymptomatic carotid
586 artery disease. *Nature Rev. Cardiology* **9**, 116-124 (2011).

587 7 Nicolaides, A. N. *et al.* Asymptomatic internal carotid artery stenosis and
588 cerebrovascular risk stratification. *J Vasc Surg* **52**, 1486-1496 (2010).

589 8 Golemati, S., Gastouniotti, A. & Nikita, K. S. Toward novel noninvasive and
590 low-cost markers for predicting strokes in asymptomatic carotid
591 atherosclerosis: the role of ultrasound image analysis. *IEEE Trans Biomed Eng*
592 **60**, 652-658 (2013).

593 9 Meairs, S. & Hennerici, M. Four-dimensional ultrasonographic
594 characterization of plaque surface motion in patients with symptomatic and
595 asymptomatic carotid artery stenosis. *Stroke* **30**, 1807-1813 (1999).

596 10 Shi, H. *et al.* Preliminary in vivo atherosclerotic carotid plaque
597 characterization using the accumulated axial strain and relative lateral shift
598 strain indices. *Phys Med Biol* **53**, 6377-6394 (2008).

599 11 Gastouniotti, A. *et al.* A novel computerized tool to stratify risk in carotid
600 atherosclerosis using kinematic features of the arterial wall. *IEEE J Biomed*
601 *Health Inform* **19**, 1137-1145 (2015).

602 12 Tat, J., Psaromiligkos, I. N. & Daskalopoulou, S. S. Carotid atherosclerotic
603 plaque alters the direction of longitudinal motion in the artery wall.
604 *Ultrasound Med Biol* **42**, 2114-2122 (2016).

605 13 Gastouniotti, A., Golemati, S., Stoitsis, J. S. & Nikita, K. S. Carotid artery wall
606 motion analysis from B-mode ultrasound using adaptive block matching: in
607 silico evaluation and in vivo application. *Phys Med Biol* **58**, 8647-8661 (2013).

608 14 Golemati, S., Gastouniotti, A. & Nikita, K. S. Ultrasound-image-based
609 cardiovascular tissue motion estimation. *IEEE Rev Biomed Engi* **9**, 208-218
610 (2016).

611 15 Cinthio, M. *et al.* Longitudinal movements and resulting shear strain of the
612 arterial wall. *Am J Physiol - Heart Circ Physiol* **291**, H394-402 (2006).

613 16 Golemati, S. *et al.* Carotid artery wall motion estimated from B-mode
614 ultrasound using region tracking and block matching. *Ultrasound Med Biol* **29**,
615 387-399 (2003).

616 17 Xu, C. *et al.* Beat-to-beat blood pressure and two-dimensional (axial and
617 radial) motion of the carotid artery wall: physiological evaluation of arterial
618 stiffness. *Sci Rep* **7**, 42254, (2017).

619 18 Zahnd, G. *et al.* Measurement of two-dimensional movement parameters of
620 the carotid artery wall for early detection of arteriosclerosis: a preliminary
621 clinical study. *Ultrasound Med Biol* **37**, 1421-1429 (2011).

622 19 Soleimani, E., Mokhtari-Dizaji, M. & Saberi, H. A novel non-invasive ultrasonic
623 method to assess total axial stress of the common carotid artery wall in
624 healthy and atherosclerotic men. *J Biomech* **48**, 1860-1867 (2015).

625 20 Svedlund, S. & Gan, L. M. Longitudinal common carotid artery wall motion is
626 associated with plaque burden in man and mouse. *Atherosclerosis* **217**, 120-
627 124 (2011).

628 21 Zahnd, G., Saito, K., Nagatsuka, K., Otake, Y. & Sato, Y. Dynamic block
629 matching to assess the longitudinal component of the dense motion field of

630 the carotid artery wall in B-mode ultrasound sequences—Association with
631 coronary artery disease. *Med Phys* **45**, 5041-5053 (2018).

632 22 Golemati, S. *et al.* Comparison of block matching and differential methods for
633 motion analysis of the carotid artery wall from ultrasound images. *IEEE Trans*
634 *Inf Technol Biomed* **16**, 852-858 (2012).

635 23 Bang, J. *et al.* A new method for analysis of motion of carotid plaques from RF
636 ultrasound images. *Ultrasound Med Biol* **29**, 967-976 (2003).

637 24 Ichinose, N. *et al.* Predicting ischemic stroke after carotid artery stenting
638 based on proximal calcification and the jellyfish sign. *J Neurosurg* **128**, 1280-
639 1288 (2018).

640 25 Kume, S. *et al.* Vulnerable carotid arterial plaque causing repeated ischemic
641 stroke can be detected with B-mode ultrasonography as a mobile
642 component: Jellyfish sign. *Neurosurg Rev* **33**, 419-430 (2010).

643 26 Ogata, T., Yasaka, M., Wakugawa, Y., Kitazono, T. & Okada, Y. Morphological
644 classification of mobile plaques and their association with early recurrence of
645 stroke. *Cerebrovasc Dis* **30**, 606-611 (2010).

646 27 Kashiwazaki, D. *et al.* Identification of high-risk carotid artery stenosis:
647 motion of intraplaque contents detected using B-mode ultrasonography. *J*
648 *Neurosurg* **117**, 574-578 (2012).

649 28 Dempsey, R. J. *et al.* Carotid atherosclerotic plaque instability and cognition
650 determined by ultrasound-measured plaque strain in asymptomatic patients
651 with significant stenosis. *J Neurosurg* **128**, 111-119 (2018).

652 29 Khan, A. A. *et al.* Noninvasive characterization of carotid plaque strain. *J Vasc*
653 *Surg* **65**, 1653-1663 (2017).

654 30 Meshram, N. H. *et al.* Quantification of carotid artery plaque stability with
655 multiple region of interest based ultrasound strain indices and relationship
656 with cognition. *Phys Med Biol* **62**, 6341-6360 (2017).

657 31 Roy Cardinal, M. H. *et al.* Carotid artery plaque vulnerability assessment using
658 noninvasive ultrasound elastography: validation with MRI. *AJR. Am J*
659 *Roentgenol* **209**, 142-151 (2017).

660 32 Wang, X. *et al.* Classification of symptomatic and asymptomatic patients with
661 and without cognitive decline using non-invasive carotid plaque strain indices
662 as biomarkers. *Ultrasound Med Biol* **42**, 909-918 (2016).

663 33 Kyriacou, E. *et al.* Carotid bifurcation plaque stability estimation based on
664 motion analysis. in *2017 IEEE 30th Int Symp Computer-Based Med Syst*
665 *(CBMS)*. 529-534.

666 34 Oppenheim, A. V. & Verghese, G. C. *Signals, Systems and Inference, Global*
667 *Edition*. (Pearson, 2017).

668 35 Gastounioti, A., Golemati, S., Stoitsis, J. & Nikita, K. S. Comparison of Kalman-
669 filter-based approaches for block matching in arterial wall motion analysis
670 from B-mode ultrasound. *Meas Sci Technol* **22**, 114008 (2011).

671 36 Rabiner, L. R. & Gold, B. *Theory and Application of Digital Signal Processing*.
672 (Prentice-Hall, 1975).

673 37 Elatrozy, T. *et al.* The effect of B-mode ultrasonic image standardisation on
674 the echodensity of symptomatic and asymptomatic carotid bifurcation
675 plaques. *Int Angiol* **17**, 179-186 (1998).

- 676 38 Zureik, M. *et al.* Echogenic carotid plaques are associated with aortic arterial
677 stiffness in subjects with subclinical carotid atherosclerosis. *Hypertension* **41**,
678 519-527 (2003).
- 679 39 Froio, A., Rossi, L., Pasquadibisceglie, S. & Biasi, G. M. Ultrasonic
680 characterization of carotid plaques and its clinical implications. in *Noninvasive*
681 *Vascular Diagnosis: A Practical Guide to Therapy* (eds Ali F. AbuRahma &
682 Dennis F. Bandyk) 157-171 (Springer London, 2013).
- 683 40 Karamizadeh, S., Abdullah, S. M., Manaf, A. A., Zamani, M. & Hooman, A. An
684 overview of principal component analysis. *J Signal Inf Process* **4**, 173-175
685 (2013).
- 686 41 Witten, I. H., Frank, E., Hall, M. A. & Pal, C. J. *Data Mining, Fourth Edition:*
687 *Practical Machine Learning Tools and Techniques*. (Morgan Kaufmann
688 Publishers Inc., 2016).
- 689 42 Breiman, L. Random forests. *Machine Learning* **45**, 5-32 (2001).
- 690 43 Haibo, H., Yang, B., Garcia, E. A. & Shutao, L. ADASYN: adaptive synthetic
691 sampling approach for imbalanced learning. in *2008 IEEE Int Joint Conf Neural*
692 *Networks IJCNN* 1322-1328.
- 693 44 Stone, M. Cross-validatory choice and assessment of statistical predictions. *J*
694 *R Stat Soc Series B Stat Methodol* **36**, 111-147 (1974).
- 695 45 Sokolova, M. & Lapalme, G. A systematic analysis of performance measures
696 for classification tasks. *Inf Process Manag* **45**, 427-437 (2009).
- 697 46 Rothwell, P. M. Current status of carotid endarterectomy and stenting for
698 symptomatic carotid stenosis. *Cerebrovasc Dis* **24**, 116-125 (2007).
- 699 47 Streifler, J. Y. Asymptomatic carotid stenosis: intervention or just stick to
700 medical therapy--the case for medical therapy. *J Neural Transm (Vienna)* **118**,
701 637-640 (2011)
- 702 48 Amancio, D. R. *et al.* A systematic comparison of supervised classifiers. *PLoS*
703 *One* **9**, e94137 (2014).
- 704 49 Gastounioti, A., Golemati, S. & Nikita, K. S. Computerized analysis of
705 ultrasound images: potential associations between texture and motion
706 properties of the diseased arterial wall. in *2012 IEEE Int Ultrasonics Symp.*
707 691-694.
- 708 50 Ma, C. & Varghese, T. Comparison of cardiac displacement and strain imaging
709 using ultrasound radiofrequency and envelope signals. *Ultrasonics* **53**, 782-
710 792 (2013).
- 711 51 Steinbuch, J. *et al.* Standard b-mode ultrasound measures local carotid artery
712 characteristics as reliably as radiofrequency phase tracking in symptomatic
713 carotid artery patients. *Ultrasound Med Biol* **42**, 586-595 (2016).
- 714 52 Zhang, Q. *et al.* Quantification of carotid plaque elasticity and intraplaque
715 neovascularization using contrast-enhanced ultrasound and image
716 registration-based elastography. *Ultrasonics* **62**, 253-262 (2015).

717

718

719 **Acknowledgments**

720 The valuable contribution of the expert clinicians of the Department of Vascular
721 Surgery, Attikon University General Hospital of Greece (Dr. C. Gkekas, Dr. N.P.E.
722 Kadoglou, Dr. J. D. Kakisis, and Dr. K. Koulia) in collecting the ultrasound image data
723 is gratefully acknowledged.

724

725

726 **Author contributions**

727 S.G., E.P., A.G. and K.S.N. designed the experiments. E.P. performed the
728 experiments. E.P., A.G., I.A. and S.G. analysed the data. C.L. overviewed recruitment
729 of subjects and collection of clinical data. S.G. and E.P. wrote the main manuscript.
730 All authors reviewed the manuscript.

731

732

733 **Additional Information**

734 **Competing Interests:** the authors declare no competing interests.

735

736

737 **Figure Legends**

738 Fig.1. Examples of interrogated ROIs and corresponding waveforms, illustrating
739 the different steps of the methodology. A – Plaque and wall ROIs in frame 1. Vertical
740 yellow dotted lines indicate the boundaries of the investigated area. The top and
741 bottom edges of the vertical yellow solid line correspond to the ROI pair for which

742 waveforms are illustrated. B – Plaque and wall ROI pixel positions at three different
743 frames representing different phases of the cardiac cycle, and corresponding time
744 points, obtained after motion analysis. Pixel positions at diastole are superimposed
745 on intermediate and systolic frames as dashed lines. C – Radial displacements of
746 selected pixels of PTS, PBS and their difference (left column), and radial
747 displacements of selected pixels of AWL, PWL and their difference, which represents
748 the arterial wall diameter (right column). D – Displacement pairs for estimation of
749 cross-correlation (top row), the corresponding cross-correlation waveforms (middle
750 row) and the selected cross-correlation segment for calculation of features (bottom
751 row). RDis: radial displacement, PRDef: plaque radial deformation, WD: wall
752 diameter, LDis: longitudinal displacement.

753 Fig. 2. Example of an echogenic (GSM=30) low-stenosis (60%) asymptomatic
754 plaque, with (a) contours superimposed on the B-mode image, illustrating the
755 distribution of CC1 values on PTS and PBS (top row), and displacement waveforms of
756 the central pixel pair and the corresponding cross-correlation waveform (bottom
757 row), (b) contours superimposed on the B-mode image, illustrating the distribution
758 of CC2 values on PTS and PBS (top row), and displacement waveforms of the central
759 pixel pair and the corresponding cross-correlation waveform (bottom row) and (c)
760 contours superimposed on the B-mode image, illustrating the distribution of CC3
761 values on PTS and PBS (top row), and displacement waveforms of the central pixel
762 pair and the corresponding cross-correlation waveform (bottom row). RDis: radial
763 displacement, PRDef: plaque radial deformation, WD: wall diameter, LDis:
764 longitudinal displacement.

765 Fig. 3. Examples of an echolucent (GSM=15) high-stenosis (70%) symptomatic
766 plaque, with (a) contours superimposed on the B-mode image, illustrating the
767 distribution of CC1 values on PTS and PBS (top row), and displacement waveforms of
768 the central pixel pair and the corresponding cross-correlation waveform (bottom
769 row), (b) contours superimposed on the B-mode image, illustrating the distribution
770 of CC2 values on PTS and PBS (top row), and displacement waveforms of the central
771 pixel pair and the corresponding cross-correlation waveform (bottom row) and (c)
772 contours superimposed on the B-mode image, illustrating the distribution of CC3
773 values on PTS and PBS (top row), and displacement waveforms of the central pixel
774 pair and the corresponding cross-correlation waveform (bottom row). RDis: radial
775 displacement, PRDef: plaque radial deformation, WD: wall diameter, LDis:
776 longitudinal displacement.
777
778

Table 1. Values of evaluation metrics for the four associations investigated, corresponding to the overall performance of all interrogated PCA-selected features.

	ACC	SENS	SPEC	PREC	NPV	F1SC	AUC
<i>Echogenicity</i>	0.73	0.73	0.73	0.88	0.51	0.80	0.81
<i>Symptomaticity</i>	0.69	0.69	0.68	0.88	0.41	0.77	0.79
<i>Stenosis degree</i>	0.85	0.86	0.81	0.92	0.68	0.89	0.89
<i>Plaque risk</i>	0.84	0.83	0.88	0.96	0.58	0.89	0.90

779

780

Table 2. Mean \pm standard deviation values and corresponding p-values of the synchronisation percentages, mean phase shift values, and statistically significant features for the three cross-correlation types, for echogenic and echolucent plaques.

	Echogenic	Echolucent	p-value
sp _{CC1}	52% \pm 24%	60% \pm 23%	0.11
sp _{CC2}	82% \pm 17%	81% \pm 15%	0.47
sp _{CC3}	77% \pm 18%	74% \pm 16%	0.22
mean _{CC1} (s)	0.42 \pm 0.20	0.40 \pm 0.19	0.83
mean _{CC2} (s)	0.20 \pm 0.15	0.26 \pm 0.15	0.05
mean _{CC3} (s)	0.30 \pm 0.18*	0.34 \pm 0.15*	0.09
median _{CC2} (s)	0.09 \pm 0.17	0.11 \pm 0.13	0.05

sp: synchronisation percentage

* indicates significant difference (p-value<0.05) with respect to mean_{CC2}

781

782

Table 3. Mean \pm standard deviation values and corresponding p-values of the synchronisation percentages, mean phase shift values, and statistically significant features for the three cross-correlation types, for asymptomatic and symptomatic plaques of high stenosis degrees.

	Asymptomatic	Symptomatic	p-value
sp _{CC1}	57% \pm 23%	53% \pm 21%	0.38
sp _{CC2}	82% \pm 15%	79% \pm 14%	0.34
sp _{CC3}	80% \pm 14%	76% \pm 19%	0.36
mean _{CC1} (s)	0.40 \pm 0.20	0.47 \pm 0.18	0.13
mean _{CC2} (s)	0.23 \pm 0.14	0.24 \pm 0.13	0.51
mean _{CC3} (s)	0.29 \pm 0.15*	0.32 \pm 0.18	0.64
max _{CC1} (s)	1.02 \pm 0.20	1.14 \pm 0.13	0.01
stdev _{CC1} (s)	0.33 \pm 0.11	0.39 \pm 0.09	0.05
max _{CC3} (s)	0.96 \pm 0.27	1.06 \pm 0.24	0.05

sp: synchronisation percentage, stdev: standard deviation

* indicates significant difference (p-value<0.05) with respect to mean_{CC2}

783

784

Table 4. Mean \pm standard deviation values and corresponding p-values of the synchronisation percentages, mean phase shift values, and statistically significant features for the three cross-correlation types, for low-stenosis and high-stenosis plaques.

	Low-stenosis	High-stenosis	p-value
sp _{CC1}	50% \pm 27%	57% \pm 23%	0.27
sp _{CC2}	85% \pm 16%	82% \pm 15%	0.14
sp _{CC3}	75% \pm 18%	80% \pm 14%	0.23
mean _{CC1} (s)	0.41 \pm 0.20	0.40 \pm 0.20	0.98
mean _{CC2} (s)	0.16 \pm 0.15	0.23 \pm 0.14	0.03
mean _{CC3} (s)	0.27 \pm 0.15*	0.29 \pm 0.15*	0.49
min _{CC1} (s)	0.03 \pm 0.07	0.02 \pm 0.08	0.03
max _{CC2} (s)	0.66 \pm 0.41	0.94 \pm 0.26	0.00
stdev _{CC2} (s)	0.19 \pm 0.13	0.29 \pm 0.12	0.00

sp: synchronisation percentage, stdev: standard deviation

* indicates significant difference (p-value<0.05) with respect to mean_{CC2}

785

786

Table 5. Mean \pm standard deviation values and corresponding p-values of the synchronisation percentages, mean values and statistically significant features for the three cross-correlation types, for low-risk and high-risk plaques.

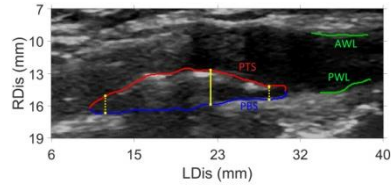
	Low-risk	High-risk	p-value
sp _{CC1}	50% \pm 27%	56% \pm 22%	0.34
sp _{CC2}	85% \pm 16%	81% \pm 15%	0.08
sp _{CC3}	75% \pm 18%	79% \pm 16%	0.36
mean _{CC1} (s)	0.41 \pm 0.20	0.41 \pm 0.20	0.79
mean _{CC2} (s)	0.16 \pm 0.15	0.23 \pm 0.14	0.02
mean _{CC3} (s)	0.27 \pm 0.15*	0.30 \pm 0.16*	0.35
min _{CC1} (s)	0.03 \pm 0.07	0.02 \pm 0.07	0.04
max _{CC2} (s)	0.66 \pm 0.41	0.94 \pm 0.27	0.00
stdev _{CC2} (s)	0.19 \pm 0.13	0.29 \pm 0.12	0.00

sp: synchronisation percentage, stdev: standard deviation

* indicates significant difference (p-value<0.05) with respect to mean_{CC2}

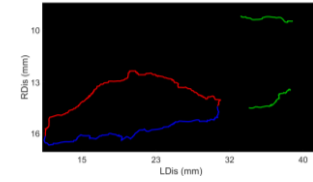
A - Selection of ROIs

Frame 1

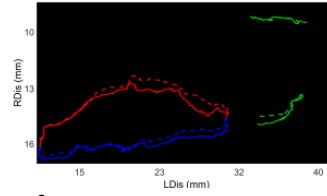


B - Motion estimation of selected ROIs

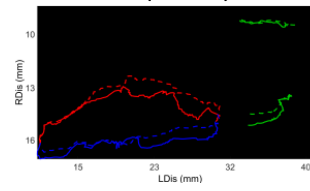
Diastolic frame
(5.32 s)



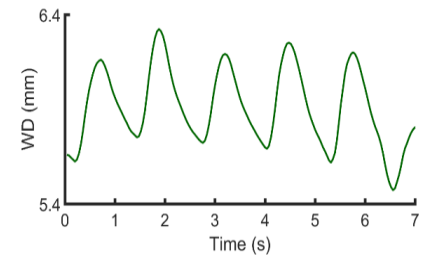
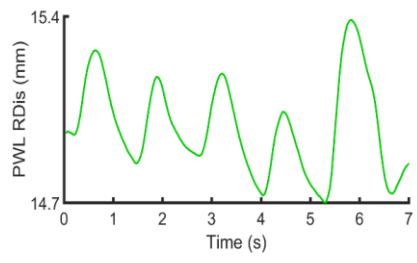
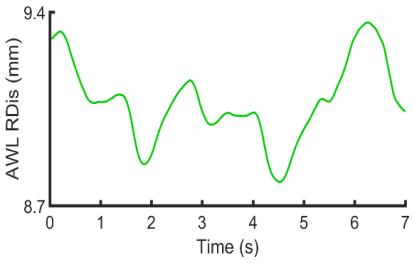
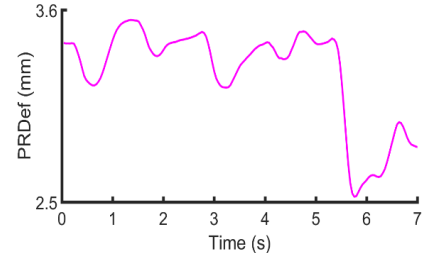
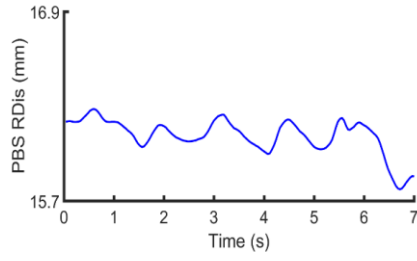
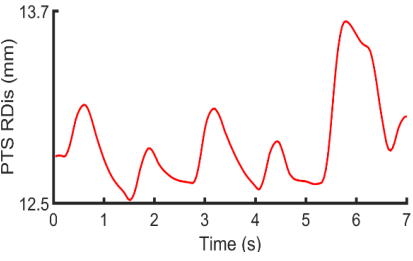
Intermediate frame
(5.56 s)



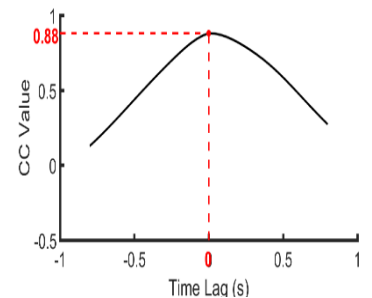
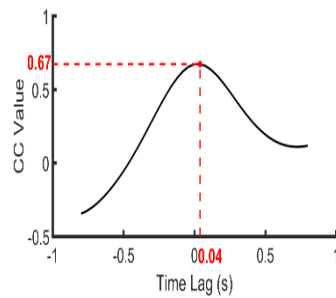
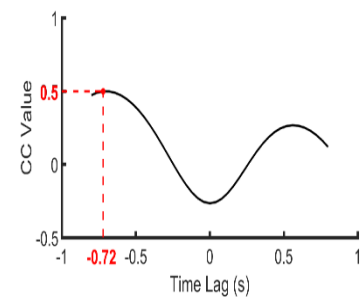
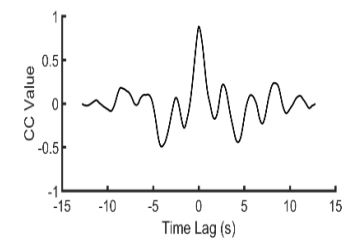
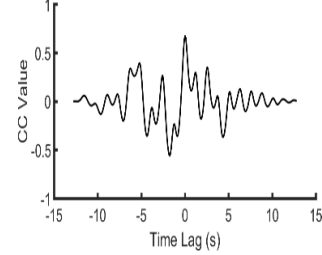
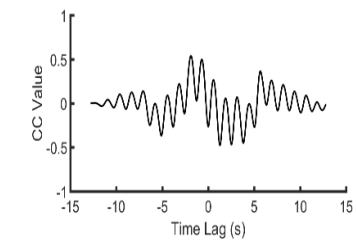
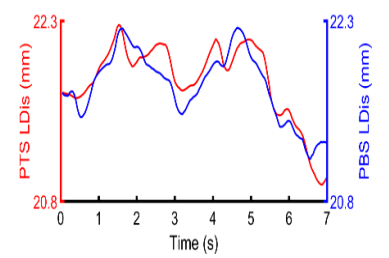
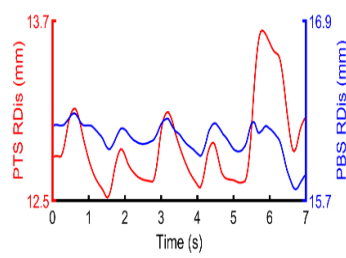
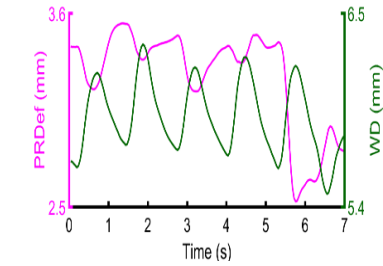
Systolic frame
(5.76 s)

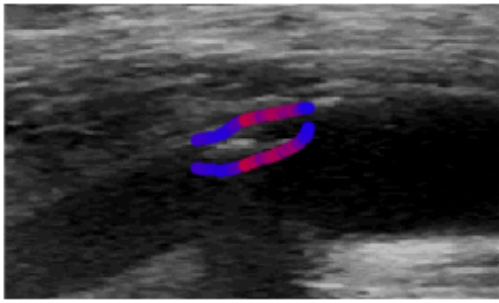


C - Examples of interrogated waveforms

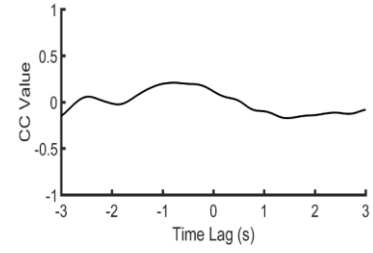
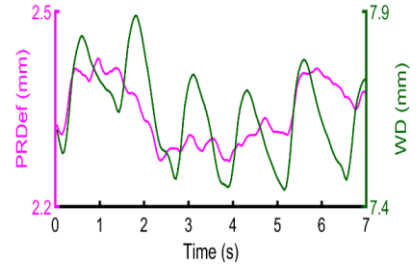


D - Examples of cross-correlation waveforms

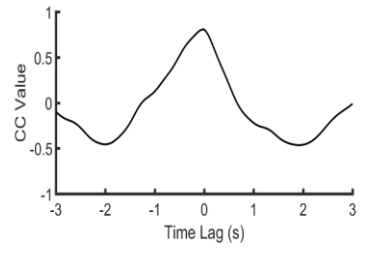
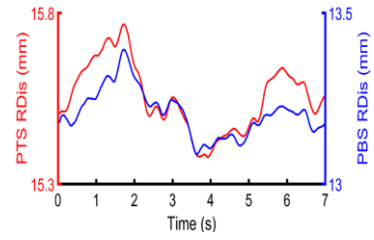




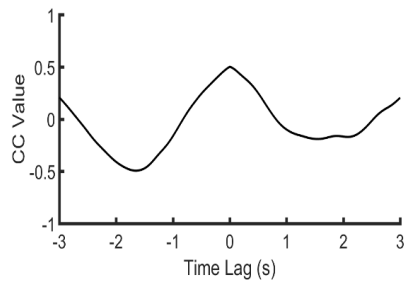
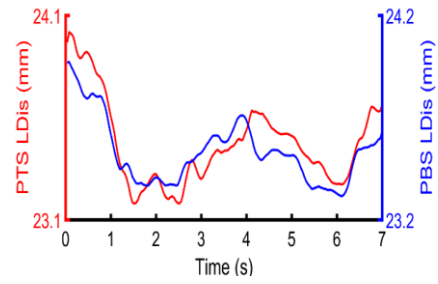
(a)

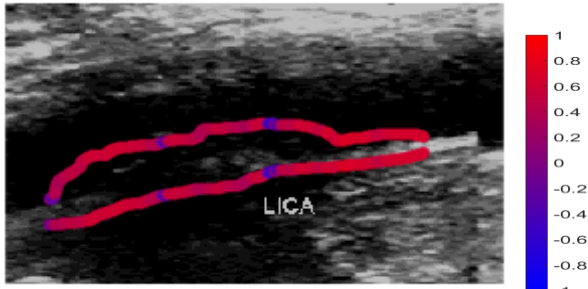


(b)

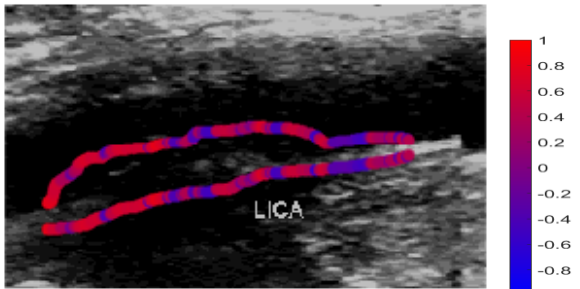
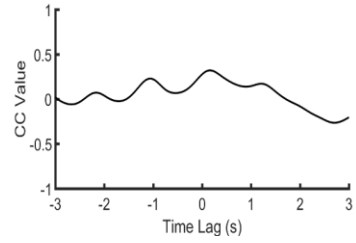
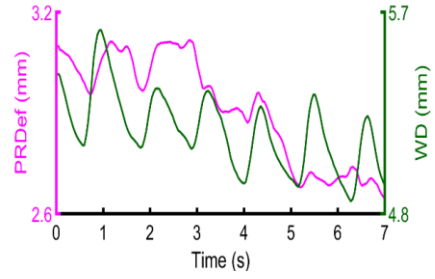


(c)

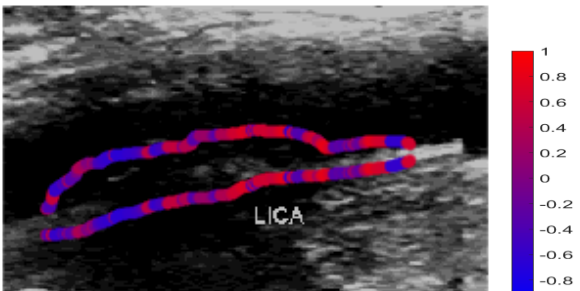
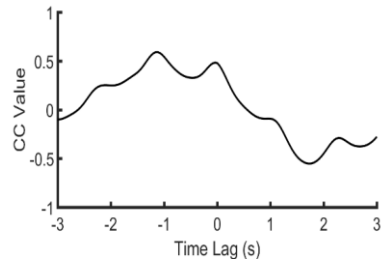
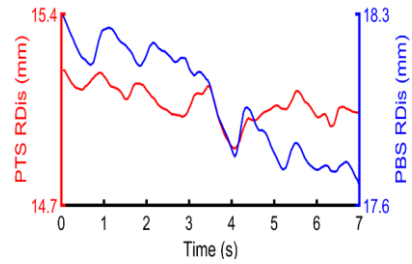




(a)



(b)



(c)

